Available online at www.sciencedirect.com
ScienceDirect
Ceramics International 37 (2011) 411–418
CERAMICS INTERNATIONAL
www.elsevier.com/locate/ceramint

Short communication

Phase composition of bauxite-based refractory castables

Morsy M. Abou-Sekkina [a,*], Salah A. Abo-El-Enein [b], Nagy M. Khalil [c], Osama A. Shalma [d]

[a] Department of Chemistry, Faculty of Science, Tanta University, Tanta, Egypt
[b] Department of Chemistry, Faculty of Science, Ain Shams University, Cairo, Egypt
[c] Refractories, Ceramics and Building Materials Department, National Research Center (NRC), Giza, Egypt
[d] Environmental Monitoring Laboratory, Tanta, Egypt

Received 24 November 2009; received in revised form 8 May 2010; accepted 30 July 2010
Available online 21 August 2010

Abstract

The bauxite-based refractory castables are composed of 90 wt.% well-graded (coarse, medium, and fine) bauxite aggregate, 10 wt.% binding matrix and adequate amount of distilled water. The binder mixture was calcium aluminate cement (CAC) containing 80% alumina and magnesium-aluminate spinel (MA-spinel) or mullite either preformed or obtained in situ.

The phase composition of the prepared castable samples was investigated by using X-ray diffraction (XRD) analysis, scanning electron microscopy, energy dispersive X-ray analysis, differential thermal analysis (DTA) and thermal gravimetric analysis.

The XRD patterns indicated the formation of the corundum phase along with mullite phase in all of bauxite-based castable samples. The scanning electron microscopy (SEM) micrographs show densely packed microstructures with an abundant of corundum grains of comparable sizes, rounded and sub-rounded, homogeneously embedded in the matrix. Some needle-shaped mullite crystals are distributed from place to place. The DTA curve of the castable samples showed three endotherms due to the release of free or the physically absorbed water, the dehydroxylation of the chemically bound water and due to some dehydration and dehydroxylation reactions.

Keywords: A. Processing hotpressing; B. Structure and microstructure electron microscopy; C. Properties mechanical properties; D. Composition mullite

1. Introduction

Refractory castables or concretes are relatively new class of refractories. They have gained wide applications during the last decades. They have the great advantage of setting and hardening quickly at room temperature so they can be used for building structures as well as for patching and coating bricks. They offer various advantages over conventional refractory bricks in terms of application rate as well as cost and flexibility, making them attractive to all other industrial users [1]. They consist of precision graded refractory grains that are gelled by means of a binder system in the materials green state. The most common binder used in castables is calcium aluminate cement (CAC). Castables are mixed with water and then installed by either pouring or pumping. Although CAC has been the main bonding agent in refractory castables for the last decades [2], the presence of lime in the castable matrix in association with silica leads to poor high-temperature properties [3]. Hence a range of lime-free castables, predominantly based on $MgO–SiO_2$, $Al_2O_3–SiO_2$ and $MgO–Al_2O_3$ bond systems, has been developed and resulted in suitable high-temperature properties via the formation of refractory compounds such as mullite ($3Al_2O_3{\cdot}2SiO_2$) and magnesium-aluminate spinel ($MgO{\cdot}Al_2O_3$) [4].

Magnesium-aluminate spinel ($MgO{\cdot}Al_2O_3$) offers a desirable and unique combination of mechanical, chemical and thermal properties both at ambient and elevated temperatures. It is hydraulically inert and does not behave as a binder [5]. MA-spinel is now extensively applied in high performance refractory castables. The conventional method of the preparation of MA-spinel is solid state sintering between high purity MgO and Al_2O_3 where the temperature needed is normally between 1200 and 1400 °C for commercial practice [6,7]. The self-forming (in situ) spinel is fabricated during service by reaction of fine magnesia (MgO) additions with alumina present in the matrix (bond) fines, often in the calcium aluminate cement. Very often small amount of microsilica is

* Corresponding author.
E-mail address: univprofdrmorsyabousekkina@yahoo.com (M.M. Abou-Sekkina).

0272-8842/$36.00
doi:10.1016/j.ceramint.2010.08.033

added to the in situ spinel bonded castable to promote hydration resistance [6,8,9].

Mullite ($3Al_2O_3$–$2SiO_2$) rarely occurs as a mineral in nature. It is a characteristic, strong and thermo-dynamically stable product in the high-temperature solid-state reaction between silica (SiO_2) and alumina (Al_2O_3) [10–13]. Mullite has recently become a candidate as a high-temperature structural material because of its good chemical stability and excellent physical properties [14–21]. In low and ultra low cement concretes (LCC and ULCC), fine silica and alumina powders, contained in their matrices, lead on firing to form in situ mullite in the bond phase as a network of needles at ≥1300 °C. The elongated needle-like mullite crystals grow and lock the structure to create a strong refractory bond system so improving the mechanical properties of the castable and strengths the microstructure of the binding matrix [22–24].

The properties of refractory concretes or castables are largely dependent upon the choice of refractory aggregate and hydraulic cement used. Thus a wide variety of aggregates are used in refractory concretes. Thus a wide variety of refractory concrete products with markedly different properties are available. In principle, all refractory grains can be used in refractory concrete as aggregates but in practice most aggregates contain mainly alumina and silica in various forms [25].

The goal of the present prepared materials is to offer mechanical, chemical and thermal resistant potential constructions for brick-lining of furnaces, boilers, crucibles, high-temperature furnace casted tubes and casted furnace chambers for industries and engineerings. They have the great advantage of setting and hardening quickly at room temperature. So they can be used for building structures as well as for batching and coating bricks. They offer various advantages over conventional refractory bricks in terms of application rate as well as cost and flexibility, making them attractive to all other industrial users.

2. Experimental procedures

The starting materials used in this investigation are: calcium aluminate cement (Alcoa, CA-25R-80% alumina), Chinese calcined bauxite aggregate, preformed MA-spinel ($MgO{\cdot}Al_2O_3$), preformed mullite ($3Al_2O_3$–$2SiO_2$), fine powdered magnesium oxide MgO (BDH), fine silica SiO_2 (≥96%) and fine powdered of calcined aluminum oxide Al_2O_3 (Alcoa).

The refractory aggregate (calcined bauxite) was well graded as 65 wt.% coarse (2.36–0.50 mm), 10 wt.% medium (0.50–0.25 mm) and 25 wt.% fine (<0.25 mm). The refractory castable samples were prepared according to the compositions represented in Table 1, where a 90 wt.% well-graded aggregate intermixed with the binding matrix and adequate amounts of distilled water according to the standard ''good ball in hand'' ASTM C-860 method. The mixed batches were then cast into cubes of 25 mm side length in steel moulds and left in their moulds at 100% relative humidity for 24 h. The samples were then demoulded and further cured for 7 days under water, followed by drying at 110 °C for 24 h. Finally the samples were subjected to firing at 1550 °C in an electric muffle furnace for a soaking time of 1 h.

Table 1
Mix composition of refractory castable batches based on calcined bauxite aggregate (B).

Sample symbol	Bauxite aggregate (wt.%)	Binding matrices		
		CAC (wt.%)	Spinel (wt.%)	
B0	90	10	0	
B1	90	8	2	Preformed spinel
B2	90	6	4	
B3	90	4	6	
B4	90	8	2	Preformed mullite
B5	90	6	4	
B6	90	4	6	
B7	90	8	2	In situ spinel
B8	90	4	4	($MgO + Al_2O_3$)
B9	90	6	6	
B10	90	8	2	In situ mullite
B11	90	4	4	($3Al_2O_3 + 2SiO_2$)
B12	90	6	6	

The refractory castable samples were characterized using X-ray diffraction (XRD) analysis where PHILIPS ''PW 1840'' diffractometer with Cu kα radiation and Ni-filter. PHILIPS ''PW 1729'' X-ray generator and PHILIPS ''PW 8203A'' recorder (at a scan speed 0.1°, 2θ from 5° to 100°, slit 0.2) are used. Selected castable samples were subjected to scanning electron microscopy (SEM). A ''JEOL JXA-840'' high resolution scanning electron microscope was used.

The 7-days cured samples were crushed (after drying), finely ground, and then subjected to differential thermal analysis (DTA) and thermal gravimetric analysis (TGA). This investigation was carried out using a ''Shimadzu DTA-50'' and ''Shimadzu TGA-50'' thermal analyzers. Each sample was heated in nitrogen atmosphere (rate flow of N_2: 20 ml/min) from the ambient temperature to 1000 °C with heating rate of 10 °C/min.

3. Results and discussion

3.1. Microstructure of the fired castables

The phase composition of the bauxite-based (B0, B2, B8, B5 and B11) castable specimens sintered at 1550 °C for 1 h, were investigated by XRD analysis and scanning electron microscope (SEM). The castable specimen B0 was taken as the control castable sample for bauxite-based castables. XRD patterns of the castable specimens B0, B2, B8, B5 and B11 are shown in Figs. 1 and 2. The XRD patterns indicated the formation of the corundum phase along with mullite phase for all of the three castable specimens. The other minor phases, CAC and spinel or its oxides, cannot be detected by XRD analysis. The SEM micrographs of the castable specimens B2, B8, B5 and B11 are shown in Figs. 3–6. The mineral phases of bauxite castable samples are essentially corundum, mullite, and glass.

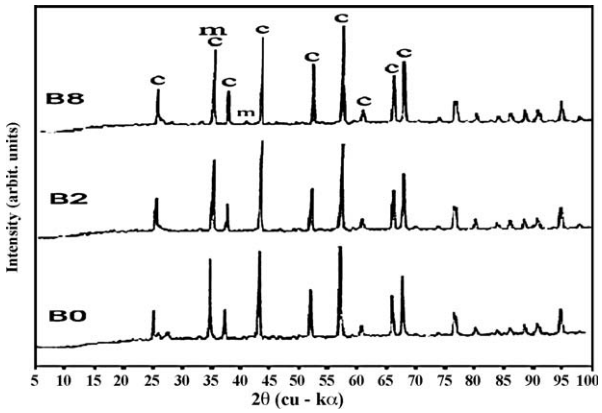

Fig. 1. X-ray diffraction patterns of castables B0, B2 and B8 fired at 1550 °C for 1 h (c: corundum, m: mullite).

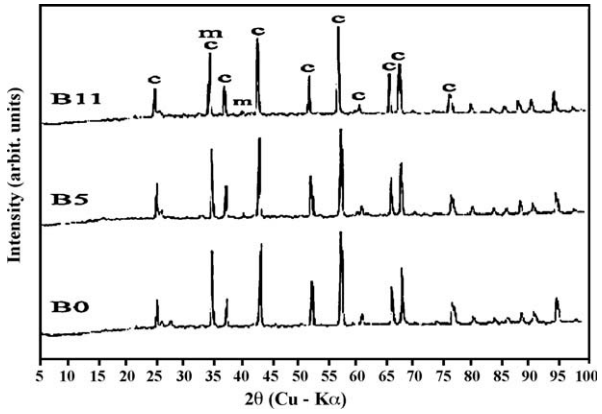

Fig. 2. X-ray diffraction patterns of castables B0, B5 and B11 fired at 1550 °C for 1 h (c: corundum, m: mullite).

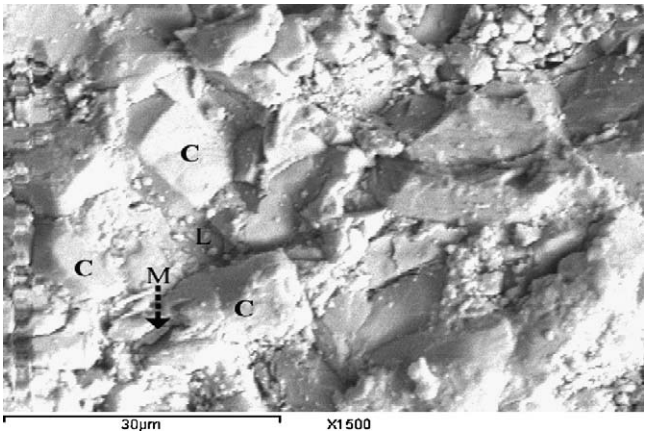

Fig. 3. SEM photomicrographs of B2 castable sample fired at 1550 °C for 1 h (C: corundum grains, M: needle-shaped mullite).

Their microstructure is mainly composed of granular corundum skeleton structure interlaced with mullite crystals (similar observations were also reported in an earlier investigation [26]). The SEM micrographs show densely packed microstructures with an abundant of corundum grains of comparable sizes, rounded and sub-rounded, homogeneously embedded in the matrix. Some needle-shaped (elongated rod) mullite crystals are also distributed from place to place. The liquid phase could also be distinguished in the matrix due to the impurities and calcium aluminate cement present in the bauxite castables (similar results were obtained in earlier publications [27–29]). Grain shapes vary from

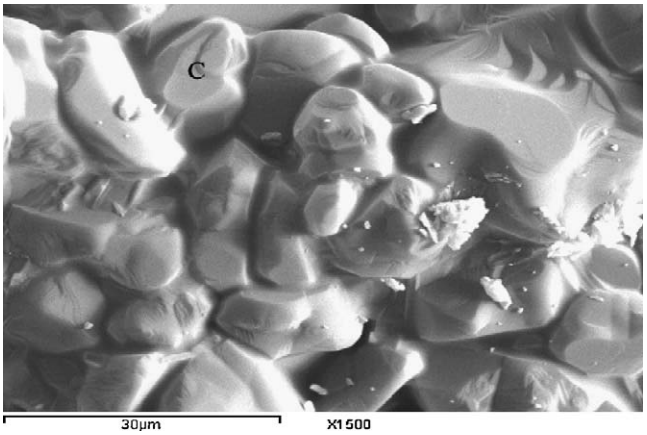

Fig. 4. SEM photomicrographs of B8 castable sample fired at 1550 °C for 1 h (C: corundum grains).

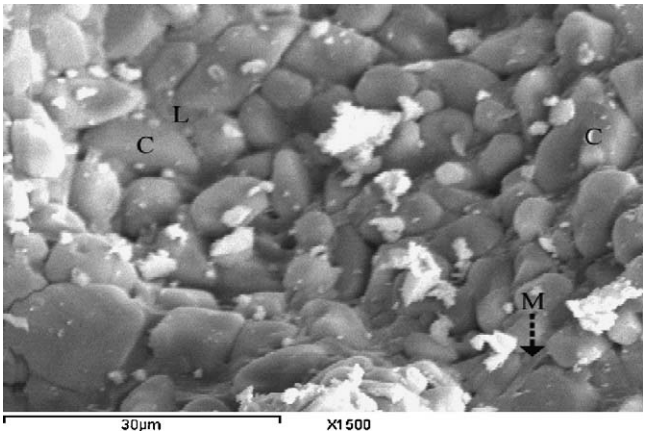

Fig. 5. SEM photomicrographs of B5 castable sample fired at 1550 °C for 1 h (C: corundum grains, M: needle-shaped mullite, L: liquid phase).

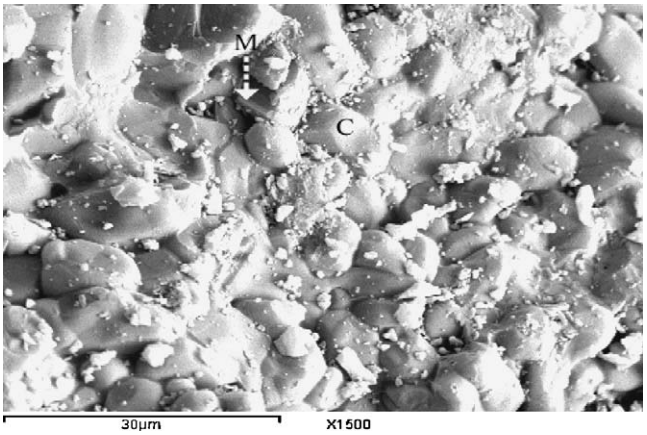

Fig. 6. SEM photomicrographs of B11 castable sample fired at 1550 °C for 1 h (C: corundum grains, M: needle-shaped mullite).

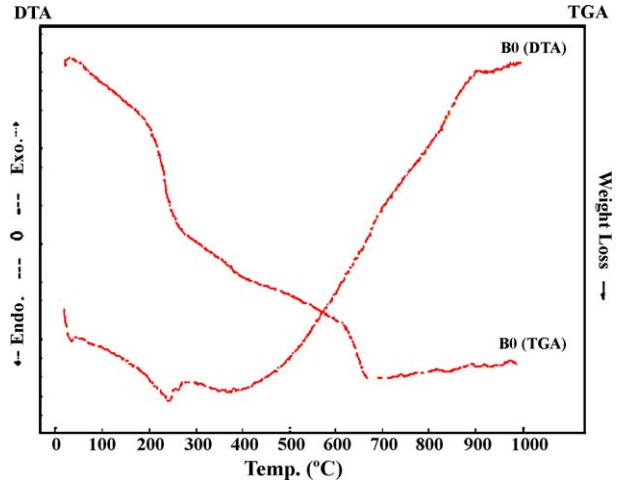

Fig. 7. Thermal analyses (TGA and DTA) of castable sample B0, hydrated for 7 days.

spherical to polyhedral nature and some pores are trapped inside the grains [27].

The corundum phase is appeared due to the transformation of bauxite minerals to corundum. This transformation occurred in two distinct steps, namely: (i) the dehydroxylation (at about 500 °C) leads to the formation of the transition phase and (ii) a sort of localized atomic rearrangement in which the tetrahedrally coordinated Al in the α-Al_2O_3 structure move to octahedrally coordinated sites in the corundum structure [30]. The presence of different impurities in bauxite versus alumina helps the formation of mullite that appeared as a result of the reaction between silica impurities and alumina in the castable samples sintered at 1550 °C [29].

3.2. Differential thermal analysis and thermal gravimetric analysis

The results of TGA and DTA of castable sample B0 (the control castable sample), hydrated for 7 days are shown in Fig. 7. Castable sample B0 displays DTA endotherms at ≈70, 241, 263 °C and broad endotherm in the region 286–695 °C. It shows broad exotherm in the region ≈700 up to 1000 °C. The TGA thermogram of the castable sample B0 is from room temperature to 1000 °C. The weight loss can be divided into stages as in Table 2. The total weight loss was 4.079% from room temperature to 700 °C.

Table 2
The percentage weight loss of castable sample B0.

Temperature stage (°C)		Castable sample B0 (sample wt.: 5.972 mg)
Start	End	Wt. loss%
26	203	0.801
205	266	1.261
266	388	0.624
388	621	0.681
621	675	0.712
Total		4.079

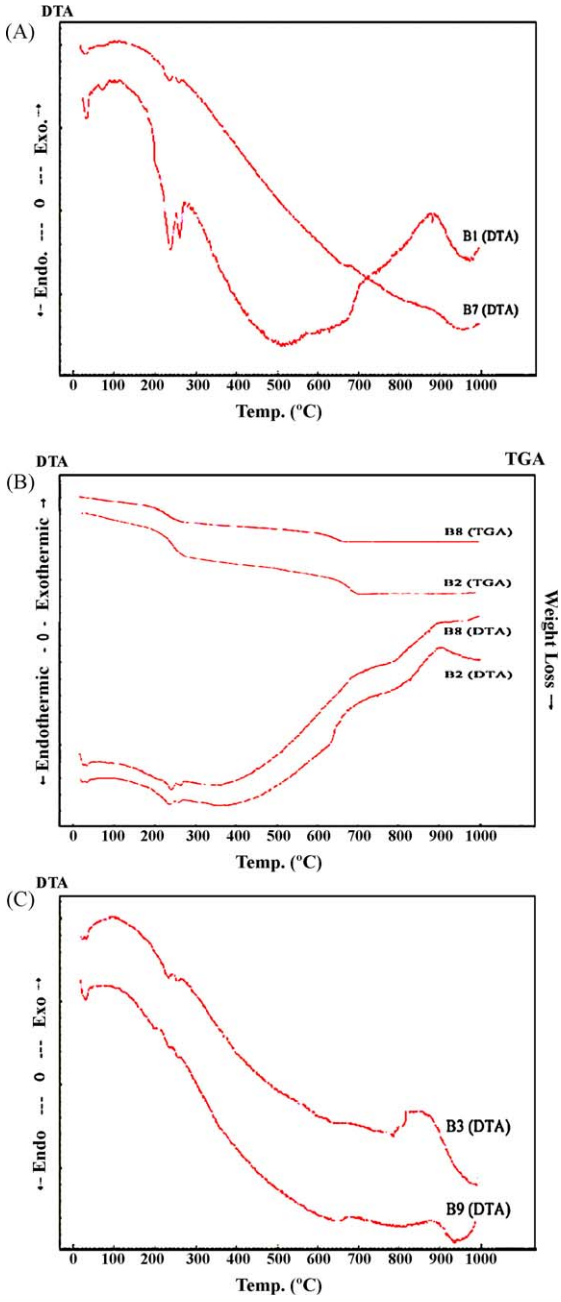

Fig. 8. Differential thermal analysis (DTA) of castable samples couples B1, B7 (A); B2, B8 (B); and B3, B9 (C), respectively.

3.2.1. Bauxite-based castable samples containing spinel (preformed or in situ)

Fig. 8A–C shows the DTA thermograms of castable samples couples (hydrated for 7 days) B1, B7; B2, B8; and B3, B9, respectively.

They show DTA endotherms at ≈35, ≈235, ≈265 °C and broad endotherms in the region ≈265–850 °C. The castable samples B2 and B8 show broad exotherm in the region ≈500 up to 1000 °C.

The TGA thermograms of the castable samples B2 and B8 are from room temperature to 1000 °C. The stages of percentage weight loss are shown in Table 3. The total weight

Table 3
The percentage weight loss of castable samples B2 and B8.

Temp stage (°C)		Castable sample B2 (sample wt.: 9.744 mg)	Temperature stage (°C)		Castable sample B8 (sample wt.: 28.21 mg)
Start	End	Wt. loss%	Start	End	Wt. loss%
31	199	0.566			–
199	283	0.918			–
283	471	0.354	270	513	1.696
472	650	0.430	514	681	0.032
652	715	0.479			
Total		2.747			1.728

loss of both castable samples was 2.75% and 1.73%, respectively, as measured from room temperature to 700 °C.

3.2.2. *Bauxite-based castable samples containing mullite (preformed or in situ)*

Fig. 9A–C shows the DTA thermograms of castable samples couples (hydrated for 7 days) B4, B10; B5, B11; and B6, B12, respectively.

They show DTA endotherms at ≈30, ≈235, ≈260 °C and broad endotherms in the region ≈260–830 °C. The castable samples B5 and B11 show broad exotherm in the region ≈500 up to 1000 °C.

The TGA thermograms of the castable samples B5 and B11 are from room temperature to 1000 °C. The stages of percentage weight loss are shown in Table 4. The total weight loss of both castable samples was 2.79% and 3.23%, respectively, as measured from room temperature to 700 °C.

The TGA and DTA of bauxite-based castable samples is mainly the thermal analysis of bauxite (the main constituent of the castable samples, 90%) that is based on the dehydroxylation of the gibbsite [α-$Al(OH)_3$] and boehmite [γ-AlO(OH)] [31].

The endotherms at 35 °C is due to endothermic reaction accompanied by weight loss as a result of the dehydration (removal) of surface coordinated and adsorbed water (the physically bound water) in the interlayer of the plates of unit lattices of the bauxite aggregate [32–35]. The substantial loss in weight at ambient to 200 °C is due to the loss of water [36].

The dehydration occurs in three stages between room temperature and ≈400 °C. The two first stages actually involve the elimination of physically absorbed water that retained in the pores and present in the binder hydrates. In the first stage, from ambient temperature to ≈100 °C, the main mechanism is evaporation of free water. As the castable continues to be heated, the second important stage begins with the ebullition of free water. The third stage occurs in the temperature range of 200 to ≈400 °C and is apparently not related to free water, but instead to hydrated products formed during the moistening of the sample [37,38].

The endotherms at 235 and 265 °C are due to the dehydroxylation (the loss of hydroxyls, i.e. chemically bound water from within the lattices) of the gibbsite. The temperature range 200–400 °C is typical for the decomposition of gibbsite ($Al(OH)_3$) and hexahydrated tricalcium aluminate ($3CaO{\cdot}Al_2O_3{\cdot}6H_2O$) [39].

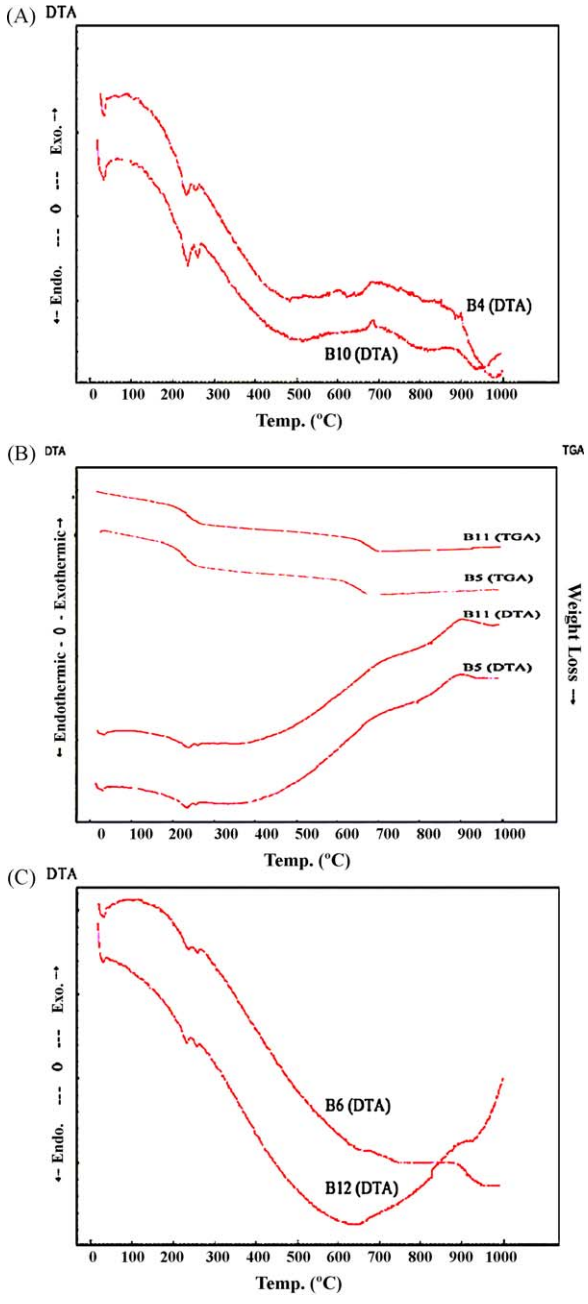

Fig. 9. Differential thermal analysis (DTA) of castable samples couples B4, B10 (A); B5, B11 (B); and B6, B12 (C), respectively.

Table 4
The percentage weight loss of castable samples B5 and B11.

Temperature stage (°C)		Castable sample B5 (sample wt.: 13.690 mg)	Temperature stage (°C)		Castable sample B11 (sample wt.: 7.876 mg)
Start	End	Wt. loss%	Start	End	Wt. loss%
34	197	0.622	27	192	0.682
197	267	0.922	193	267	0.998
269	596	0.585	267	448	0.421
598	687	0.661	450	638	0.475
			638	701	0.655
Total		2.790			3.231

Dehydroxylation of gibbsite starts around 220 °C and is complete around 350 °C [36]; and the broad endotherms in the range ≈270–700 °C are due to the dehydroxylation of boehmite [32,34]. Dehydroxylation of boehmite was observed to commence around 250 °C [36].

The elimination of physically combined water is the main cause of weight loss at temperatures approaching 100 °C (at ambient pressure). The decomposition of hydrates and gels, on the other hand, occurs according to complex kinetics at temperatures ranging from 100 to 550 °C and above, releasing a specific number of water molecules in proportion to the degraded phase [40].

The broad exotherms in the region ≈700 up to 1000 °C are a result of lattice rearrangement due to heat capacity and/or phase transition to corundum. The exotherm at 900–1000 °C reflects the formation of crystalline product from the amorphous intermediate phase. Upon further heating, sintering reactions took place and mullite formation, γ-alumina and cristoballite (SiO_2) are observed [35,41–43].

Dehydroxylation is accompanied by a continuous weight loss [44]. During this stage, the water vapor is evolved from the dehydroxylation of gibbsite and boehmite passing through several intermediate phases until the stable high temperature rhombohedral structure, α-Al_2O_3 is formed. The initial step in the thermal reaction is the diffusion of protons and the reaction with hydroxyl ions to form water [45]. This process decomposes the binding forces between subsequent units in the gibbsite structure and causes changes in the chemical composition and density. Differential thermal analysis of a coarse-grained gibbsite has shown the presence of an endotherm around 230 °C followed by a second endotherm around 280 °C [46]. This latter endotherm is attributed to the formation of boehmite via a hydrothermal reaction due to the retarded diffusion of water out of the larger gibbsite particles. There is general agreement that boehmite and a disordered transition alumina (γ-alumina) are formed upon the thermal treatment of coarse gibbsite up to 400 °C [36]. The low temperature endotherms (at 235 and 265 °C) were attributed to non-hydrogen bonded ''outer'' hydroxyl groups that are easily removed [47]. The latter endotherm was attributed to the formation of boehmite under hydrothermal conditions due to the retarded diffusion of water out of the larger gibbsite grains [36]. The dehydroxylation in the boehmite starts at ≈480 °C and is complete by ≈520 °C. The natural boehmite is crystalline. Such difference in morphology may contribute to the differences in the observed temperatures of the dehydroxylation. It is concluded that the dehydroxylation is generally completed at 550 °C [36]. The net equation for the complete conversion is:

$$2Al(OH)_3(s) \rightarrow Al_2O_3(s) + 3H_2O(g)$$

Also in this interval (300–950 °C), the main hydration phases formed during the reaction between alumina cement and the water CAH_{10}, C_2AH_8, C_3AH_6 and AH_3 are dehydrated [48]. The endothermic effect between 250 and 350 °C showed the presence of C_3AH_6 [49]. The results explained by dehydration scheme of cement mineral hydrates [50] are as follow:

$$CAH_{10} \rightarrow C_2AH_8 + AH_3;$$

$$C_2AH_8 + AH_3 \rightarrow C_3AH_6 + 2AH_3;$$

$$C_3AH_6 + 2AH_3 \rightarrow C_{12}A_7 + CA + H\uparrow.$$

The amount of $C_{12}A_7$ increases when the specimens fired at the temperatures 600–900 °C and decreases after 950 °C. The decrease of $C_{12}A_7$ after firing at 900 °C may be explained by the intensive reaction of CA. The formula of the reaction is as follows [50]:

$$C_{12}A_7 + 5A \rightarrow 12CA.$$

4. Conclusions

The main conclusions derived from these investigations are summarized as follows:

(1) X-ray diffraction and scanning electron microscopy

The XRD patterns of the bauxite-based castable samples indicated the formation of the corundum phase along with mullite phase in all of them. The other minor phases, CAC and additive (added spinel or mullite or their oxides); cannot be detected by XRD analysis. The SEM micrographs show densely packed microstructures with an abundant of corundum grains of comparable sizes, rounded and sub-rounded, homogeneously embedded in the matrix. Some needle-shaped mullite crystals are distributed. The matrix also has some of liquid phase due to the impurities and high alumina cement present in the bauxite castables.

(2) The thermal analyses (TGA) and (DTA)

The thermal analyses by (TGA) and (DTA) measurements of bauxite-based castable samples containing spinel and mullite (preformed or in situ) are mainly the thermal analysis of bauxite (the main constituent of the castable samples, 90 wt.%) that is based on the dehydroxylation of the gibbsite [α-$Al(OH)_3$] and boehmite [γ-AlO(OH)]. The differential thermal analyses (DTA) and thermogravimetric (TGA) measurements of kaolin-based castable samples containing spinel and mullite (preformed or in situ) are mainly the thermal analysis of kaolin (the main constituent of the castable samples, 90 wt.%). In general, the DTA curve of each bauxite-based castable sample shows three endotherms in the temperature range between room temperature and ≈265 °C and broad endotherm in the region ≈265–800 °C. The first one is due to the release of free or the physically absorbed water in the interlayer of between the plates of unit lattices of the bauxite aggregate. The second and third endotherms are due to the dehydroxylation of the chemically bound water from within the lattices) of gibbsite. The broad endotherms are due to the dehydroxylation of boehmite. Also in this interval (300–950 °C), the main hydration phases formed during the reaction between alumina cement and the water CAH_{10}, C_2AH_8, C_3AH_6 and AH_3 are dehydrated.

Results indicated that the major goal of the articles is attained at. This together with the firing condition chosen produced a final translucent and bright appearance bodies.

References

[1] L. Girgis, S. El-Hemaly, N. Khalil, Tile Brick Int. 16 (4) (2000) 250–256.

[2] W. Lee, W. Vieira, S. Zhang, K. Ahari, H. Sarpoolaky, C. Parr, Castable refractory concretes'', Int. Mater. Rev. 46 (3) (2001) 145–167.

[3] Y. Ko, Influence of micro silica addition on the properties of alumina-spinel castables, in: Proceedings of the Unified International Technical Conference on Refractories (UNITECR' 99), Berlin, Germany, (1999), pp. 22–25.

[4] F. Cunha, R. Bradt, Electric Furnace Conference Proceedings, 1999, pp. 143–152.

[5] M. Jung, Properties and uses of refractory cements developed in GDR, Silikatte Technick 27 (7) (1976) 224–226.

[6] M. Fuhrer, A. Hey, W. Lee, Microstructural evolution in self-forming spinel/calcium aluminate-bonded castable refractories, J. Eur. Ceram. Soc. 18 (15) (1998) 813–821.

[7] S. Mukhopadhyay, S. Sen, T. Maiti, M. Mukherjee, R. Nandy, B. Sinha-mahapatra, In situ spinel bonded refractory castable in relation to co-precipitation and sol–gel derived spinel forming agents, Ceram. Int. 29 (8) (2003) 857–868.

[8] Y. Ko, Influence of the characteristics of spinels on the slag resistance of Al_2O_3–MgO and Al_2O_3–spinel castables, J. Am. Ceram. Soc. 83 (9) (2000) 2333–2335.

[9] C. Parr, T. Beir, M. Vialle, C. Revais, An approach to formulate spinel forming castables, in: Proceedings of the Unified International Technical Conference on Refractories (UNITECR' 99), Berlin, Germany, (1999), pp. 19–21.

[10] W. Kronert, U. Schumacher, Use of low-cement and ultralow-cement refractory castables in the iron and steel industry furnace prospects, Interceram. (Aachen Proc. 1988) 3 (8) (1989) 12–18.

[11] A. Hundere, B. Myhre, Effect of different finest fractions (SiO_2 and Al_2O_3) in alumina based ultra low cement castables, in: Elkem Refractories, Presented at the Amer. Ceram. Soc. 98th Annual Meeting in Indianapolis, 1996.

[12] Y. Pivinski, New refractory concretes and binding systems, Refract. Ind. Ceram. 39 (314) (1998) 91–99.

[13] S. Moehmel, W. Gessner, A. Bier, C. Parr, The influence of micro silica on the course of hydration of mono-calcium aluminate, in: Proc. Inter. Conf., Calcium Aluminate Cements, IOM Communications, London, 2001, pp. 319–330.

[14] K. Mazdiyasni, L. Brown, Synthesis and mechanical properties of stoichiometric aluminum silicate (mullite), J. Am. Ceram. Soc. 55 (1972) 548.

[15] B. Ghate, D. Hasselman, R. Spriggs, Synthesis and characterization of high purity, fine grained mullite, Am. Ceram. Soc. Bull. 52 (9) (1973) 670–672.

[16] W. Cameroon, Miner. Am. 62 (1977) 747.

[17] N. Tamari, I. Kondoh, T. Tanaka, H. Katsuki, Mechanical properties of alumina–mullite composites, J. Ceram. Soc. Jpn. 101 (1993) 721.

[18] H. Schneider, K. Okada, J. Pask, Mullite and Mullite Ceramics, J. Wiley & Sons, New York, NY, 1994, pp. 153–160.

[19] D. Ibrahim, S. Naga, Z. Kader, E. Salam, Cordierite–mullite refractories, Ceram. Int. 21 (1995) 265–269.

[20] X. Zhong, G. Sun, Z. Kader, E. Salam, Thermomechanical properties of corundum–mullite–zirconia materials, in: Proceedings of the Unified International Technical Conference on Refractories (UNITECR' 97), New Orleans, USA, (1997), pp. 943–952.

[21] T. Takei, Y. Kameshima, A. Yasumori, K. Okada, Crystallization kinetics of mullite in alumina–silica glass fibers, J. Am. Ceram. Soc. 82 (10) (1999) 2876–2880.

[22] B. Myhre, Strength development of bauxite-based ultralow-cement castables, Am. Ceram. Soc. Bull. 73 (5) (1994) 68–73.

[23] B. Sandburg, B. Myhre, Castables in the system MgO–Al_2O_3–SiO_2, in: Proceedings of the Unified International Technical Conference on Refractories (UNITECR' 95), Kyoto, Japan, (1995), pp. 173–179.

[24] M. Hundere, B. Myhre, Substitution of reactive alumina with microsilica in low cement and ultra low cement castables, in: Proceedings of the Unified International Technical Conference on Refractories (UNITECR' 97), New Orleans, USA, (1997), pp. 91–100.

[25] L. Girgis, S. El-Hemaly, N. Khalil, Int. Ceram. 52 (3) (2003) 40–44.

[26] F. Ye, M. Rigaud, X. Liu, X. Zhong, High temperature mechanical properties of bauxite-based SiC-containing castables, Ceram. Int. 30 (2004) 801–805.

[27] S. Mukhopadhyay, S. Ghosh, M. Mahapatra, R. Mazumder, P. Barick, S. Gupta, S. Chakraborty, Easy-to-use mullite and spinel sols as bonding agents in a high-alumina based ultra low cement castable, Ceram. Int. 28 (7) (2002) 719–729.

[28] N. Khalil, Refractory concrete based on barium aluminate–barium zirconate cements for steel-making industries, Ceram. Int. 31 (2005) 937–943.

[29] M. Zawrah, Effect of zircon additions on low and ultra-low cement alumina and bauxite castables, Ceram. Int. 33 (5) (2007) 751–759.

[30] J. Garcia-Guinea, V. Correcher, J. Rubio, F. Valle-Fuentes, Effects of preheating on diaspore: modifications in color centers, structure and light emission, J. Phys. Chem. Solids (2005) [PCS 3773-25/5/2005-149499–XML MODEL 5, pp. 1–8].

[31] S. Goldberg, J. Davis, J. Hem, The surface chemistry of aluminum oxides and hydroxides, in: G. Sposito (Ed.), The Environmental Chemistry of Aluminum, 2nd edition, Lewis publishers, CRC Press, Inc., 1996(Chapter 7).

[32] S. Fisher, A. Fanaff, L. Picking, Landslides of southeastern Ohio, Ohio J. Sci. 68 (2) (1968) 65.

[33] D. Todor, Thermal Analysis of Minerals, Abacus Press, Tunbridge Wells, Kent, 1976, p. 256.

[34] R. Frost, J. Kloprogge, S. Russell, J. Szetu, Dehydroxylation and structure of alumina gels prepared from trisecbutoxyaluminium, Thermochim. Acta 329 (1) (1999) 47–56.

[35] S. Sayin, Origin of kaolin deposits: evidence from the Hisarcik (Emet-Kutahya) deposits, Western Turkey, Turkish J. Earth Sci. 16 (2007) 77–96.

[36] J. Kloprogge, H. Ruan, R. Frost, Thermal decomposition of bauxite minerals: infrared emission spectroscopy of gibbsite, boehmite and diaspore, J. Mater. Sci. 37 (6) (2002) 1121–1129.

[37] M. Innocentini, F. Cardoso, M. Akyioshi, V. Pandolfelli, Drying stages during the heating of high-alumina, ultra-low-cement refractory castables, J. Am. Ceram. Soc. 86 (7) (2003) 1146–1148.
[38] M. Innocentini, M. Miranda, F. Cardoso, V. Pandolfelli, Vaporization processes and pressure buildup during dewatering of dense refractory castables, J. Am. Ceram. Soc. 86 (9) (2003) 1500–1503.
[39] N. Schmitt, J. Hernandez, V. Lamour, Y. Berthaud, P. Meunier, J. Pourier, Coupling between kinetics of dehydration, physical and mechanical behaviour of high alumina castable, Cem. Concr. Res. 30 (2000) 1597–1607.
[40] M. Innocentini, A. Studart, R. Pileggi, V. Pandolfelli, PSD effect on the permeability of refractory castables, Am. Ceram. Soc. Bull. 80 (5) (2001) 31–36.
[41] J. Lemaitre, A. Lronard, B. Delmon, Le mecanisme de transformation thermique de la metakaolinite, Bull. Miner. 105 (1982) 501–507.
[42] B. Sonuparlak, M. Sarikaya, I. Aksay, Spinel phase formation during the 980 °C exothermic reaction in the Kaolinite-to-Mullite reaction series, J. Am. Ceram. Soc. 70 (11) (1987) 837–842.
[43] C. Ward, D. French, Analysis and significance of mineral matter in coal, in: 21st Annual Meeting of The Society for Organic Petrology, The University of New South Wales, Sydney, New South Wales, Australia, 2004.
[44] M. Gorea, F. Kristaly, D. Pop, Characterization of some kaolines in relationship with electric insulator ceramics microstructure, Acta Mineralogica-Petrographica Szeged 46 (2005) 9–14.
[45] F. Freund, Ber. Deut. Keram. Ges. 44 (1967) 241.
[46] C. Colombo, A. Violante, Clays, Clay Miner. 44 (1996) 113.
[47] R. Frost, J. Kloprogge, S. Russell, J. Szetu, Appl. Spectrosc. 53 (1999) 423.
[48] S. Majumdar, R. Sarkar, P. Vajifdar, R. Narayanan, S. Cursetji, A. Chatterjee, User Friendly High Refractory Calcium Aluminate Cement Proceedings of the International Conference of Calcium Aluminate Cements, Edinburg, Scotland, UK, (2001), pp. 467–476.
[49] V. Ramachandran, R. Feldman, P. Sereda, Application of differential thermal analysis in cement research, Research Paper No. 249 of the Division of Building Research, National research Council Canada, and Highway Research Record no. 62, Highway Research Board, Washington, DC, U.S.A., 1964, pp. 40–61.
[50] C. George, Aspects of calcium aluminate cement hydration, in: Proceedings of XIII Annual Symposium on Refractories Sheraton-West Port Inn St. Louis, Missouri, 1994, pp. 1–21.